

Accurate determination of black-body radiation shift, magic and tune-out wavelengths for the $6S_{1/2} \rightarrow 5D_{3/2}$ clock transition in Yb^+

A. Roy^{1,2}, S. De^{1,2}, Bindiya Arora³, and B. K. Sahoo⁴

¹CSIR-National Physical Laboratory, Dr. K. S. Krishnan Marg, New Delhi-110012, India.

²Academy of Scientific and Innovative Research, CSIR- National Physical Laboratory Campus, New Delhi, India.

³Department of physics, Guru Nanak Dev university, Amritsar, Punjab-143005, India.

⁴Atomic, Molecular and Optical Physics Division, Physical Research Laboratory, Navrangpura, Ahmedabad-380009, India.

E-mail: royatish8@gmail.com

December 2016

Abstract. We present precise values of the dipole polarizabilities (α) of the ground $[4f^{14}6s] \ ^2S_{1/2}$ and metastable $[4f^{14}5d] \ ^2D_{3/2}$ states of Yb^+ , that are **important** in reducing systematics in the clock frequency of the $[4f^{14}6s] \ ^2S_{1/2} \rightarrow [4f^{14}5d] \ ^2D_{3/2}$ transition. The static values of α for the ground and $[4f^{14}5d] \ ^2D_{3/2}$ states are estimated to be $9.8(1) \times 10^{-40} \text{ Jm}^2\text{V}^{-2}$ and $17.6(5) \times 10^{-40} \text{ Jm}^2\text{V}^{-2}$, respectively, while the tensor contribution to the $[4f^{14}5d] \ ^2D_{3/2}$ state as $-12.3(3) \times 10^{-40} \text{ Jm}^2\text{V}^{-2}$ compared to the experimental value $-13.6(2.2) \times 10^{-40} \text{ Jm}^2\text{V}^{-2}$. This corresponds to the differential scalar polarizability value of the above transition as $-7.8(5) \times 10^{-40} \text{ Jm}^2\text{V}^{-2}$ in contrast to the available experimental value $-6.9(1.4) \times 10^{-40} \text{ Jm}^2\text{V}^{-2}$. This results in the black-body radiation (BBR) shift of the clock transition as $-0.44(3) \text{ Hz}$ at the room temperature, which is large as compared to the previously estimated values. Using the dynamic α values, we report the tune-out and magic wavelengths that could be of interest to subdue systematics due to the Stark shifts and for constructing lattice optical clock using Yb^+ .

1. Introduction

Ytterbium-ion (Yb^+) is a unique system as its two quadrupole (E2) transitions, $[4f^{14}6s] \ ^2S_{1/2} \rightarrow [4f^{14}5d] \ ^2D_{3/2}$ and $[4f^{14}6s] \ ^2S_{1/2} \rightarrow [4f^{14}5d] \ ^2D_{5/2}$, and one octupole (E3) transition, $[4f^{14}6s] \ ^2S_{1/2} \rightarrow [4f^{13}6s^2] \ ^2F_{7/2}$, as shown in Fig. 1 are being undertaken for the optical frequency standards [1, 2, 3, 4, 5]. The $[4f^{14}6s] \ ^2S_{1/2} \rightarrow [4f^{14}5d] \ ^2D_{3/2}$ transition in Yb^+ has also been considered for probing parity nonconservation effect [6]. Since the $[4f^{14}6s] \ ^2S_{1/2} \rightarrow [4f^{13}6s^2] \ ^2F_{7/2}$ transition is strongly sensitive to variation of the fine structure constant (α_e) than the $[4f^{14}6s] \ ^2S_{1/2} \rightarrow [4f^{14}5d] \ ^2D_{3/2}$ transition in Yb^+ [7, 8], combining ratio of frequencies of these clock transitions with the clock

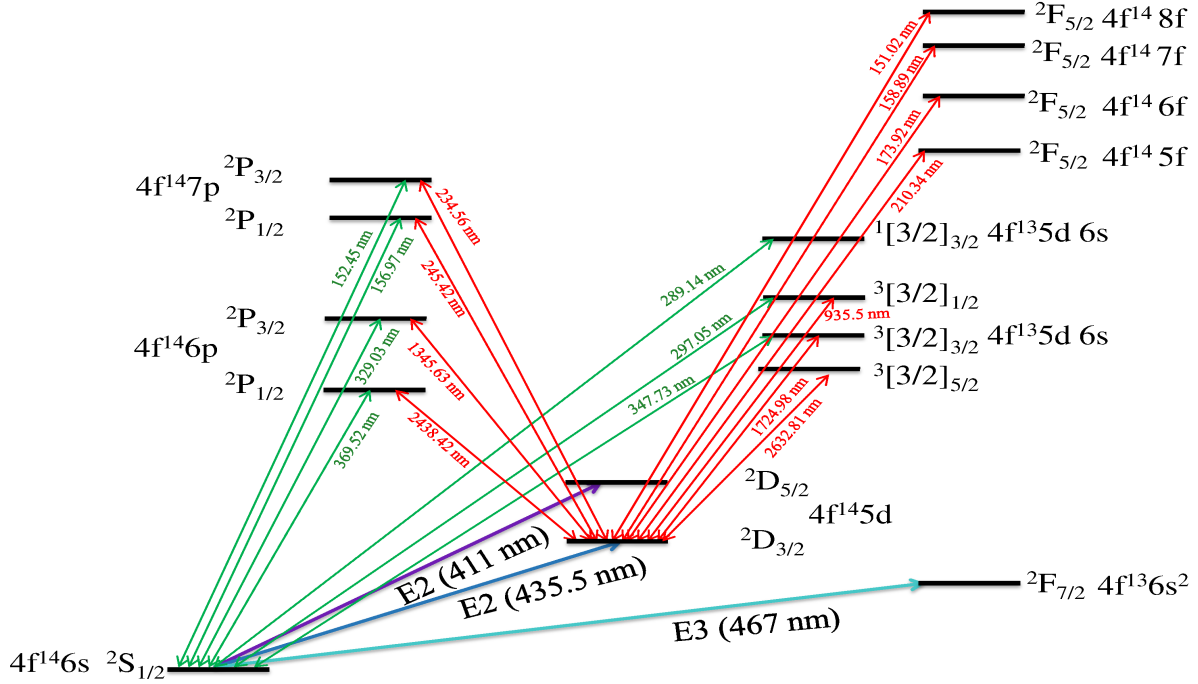


Figure 1. Energy level diagram of Yb⁺: All the clock transitions and low-lying states that are relevant for the experimental set-up and demonstrating role of their importance in calculating dipole polarizabilities of the $[4f^{14}6s] \ ^2S_{1/2}$ and $[4f^{14}5d] \ ^2D_{3/2}$ states are highlighted here.

frequencies of Cs atom and combined frequencies of Hg⁺ and Al⁺ ions, limits on the variations of α_e and proton-to-electron mass ratio are inferred [9]. In fact, all of the clock transitions in Yb⁺ seem to be sensitive to investigating possible Lorentz symmetry violation [10]. Owing to long lifetime of the $[4f^{13}6s^2] \ ^2F_{7/2}$ state (≥ 6 years), it makes the $[4f^{14}6s] \ ^2S_{1/2} \rightarrow [4f^{13}6s^2] \ ^2F_{7/2}$ transition highly forbidden and most suitable for the optical clock. On the other hand, lifetimes of the $[4f^{14}5d] \ ^2D_{3/2}$ and $[4f^{14}5d] \ ^2D_{5/2}$ states are about 55 ms and 7 ms, respectively [11, 12]. Hence, they are also suitable for the optical clocks.

Optical atomic clocks are realized in two different ways. First, in which the neutral atoms are localized in optical lattice and in the other a singly charged ion is confined in a Paul trap. Optical lattice clocks are capable of offering better statistics owing to their large signal-to-noise ratio compared to a single trapped ion clock. In contrast, using the sophisticated cooling and trapping techniques, a trapped singly charged ion can be isolated from the environmental perturbations which then acquires long coherence time to the first order. Thereby, systematics of the measured clock frequencies can be efficiently controlled and estimated in trapped ions, making them suitable contenders for the optical atomic clocks [13]. Precise measurements of the differential black-body radiation (BBR) shifts, which are crucial factors in deciding the uncertainties

of the clock transitions, are extremely challenging. Analogously accurate estimates of these quantities demand for reliable knowledge of the scalar components of the static polarizabilities. Since precise values of the static scalar polarizabilities of the atomic states associated with the $[4f^{14}6s] \ ^2S_{1/2} \rightarrow [4f^{14}5d] \ ^2D_{3/2}$ clock transition in Yb^+ are lacking, uncertainty in the BBR shift of this transition is not known [14, 15, 16]. Besides, consideration of ions in an optical lattice would be of interest for carrying out precise measurements on them as has been suggested in [17]. Few ions have already been considered for experimental investigation either in an optical dipole trap or in an optical lattice. For example, optical dipole trapping of Mg^+ at the laser wavelength of 280 nm loaded in a linear Paul trap was demonstrated for experimental implication of the quantum simulations [18]. The same group have also reported an 1D optical lattice immersed in a 3D optically trapped Mg-ions to explore their quantum dynamics [19]. Optical lattice of Yb^+ at the wavelength 377.2 nm has been experimentally demonstrated for controlling their spin motion couplings [20, 21]. Adeptness of a trapped atomic system is enhanced by using optical lattice operating at magic wavelengths (λ_{magic}), where the differential Stark shift of a given transition is effectively nullified when the lattice lasers are applied to the atomic systems. This was first demonstrated by Katori *et. al.* for neutral Sr atoms [22], following this a number of experimental and theoretical works have been carried out in other neutral atoms [23, 24, 25]. However, measurement of λ_{magic} at 395.7992(7) nm and 395.7990(7) nm in the $^{40}\text{Ca}^+$ have been reported recently [17]. After that these values have been investigated theoretically in other alkaline-earth ions [26]. Similarly, the Stark shift of an energy level is zero at the tune-out wavelengths (λ_{T}) so the atomic systems can be free from the systematics due to the Stark shifts if they are trapped using lasers at these values. Measurements of the tune-out wavelengths may be used as high-precision benchmark tests of theory [27]. Moreover, it is possible to combine measurements of magic wavelengths and lightshifts with high accuracy theoretical calculations to infer the values of some of the E1 matrix elements which are difficult to measure otherwise [17, 28, 29].

In this article, we present accurate values of the static and dynamic dipole polarizabilities of the $[4f^{14}6s] \ ^2S_{1/2}$ and $[4f^{14}5d] \ ^2D_{3/2}$ states in $^{171}\text{Yb}^+$. For their evaluations, we have used known electric dipole (E1) matrix elements extracted from the measurements of the lifetimes of some of the low-lying atomic states calculated elsewhere using the relativistic coupled-cluster (RCC) method. We have estimated core correlation effects and other contributions employing other variants of relativistic many-body methods. Using these polarizabilities, we determine the BBR shift, tune-out and magic wavelengths of the $[4f^{14}6s] \ ^2S_{1/2} - [4f^{14}5d] \ ^2D_{3/2}$ clock transition in $^{171}\text{Yb}^+$. The BBR shift of this clock transition is calculated as $-0.44(3)$ Hz at the 300 K. We also found several magic and tune-out wavelengths, among which suitable choices can be made for performing different high-precision experiments depending on their applications and availability of the lasers with the required power.

2. Theory

The Stark shift in the energy level of the n^{th} hyperfine level with angular momentum F_n and its magnetic component M_{F_n} placed in an uniform oscillating electric field of a laser beam $\mathcal{E}(t) = \frac{1}{2}\mathcal{E}\hat{\epsilon}e^{-(\omega t + \mathbf{k}\cdot\mathbf{r})} + c.c.$, with \mathcal{E} being the amplitude, $\hat{\epsilon}$ is the polarization vector of the electric field and *c.c.* referring to the complex conjugate of the former term, oscillating at frequency ω is given by

$$\Delta E_{F_n}^{\text{Stark}} \approx -\frac{1}{4}\alpha_{F_n}(\omega)\mathcal{E}^2, \quad (1)$$

where $\alpha_{F_n}(\omega)$ is the frequency dependent or dynamic polarizability of the state and given by

$$\begin{aligned} \alpha_{F_n}(\omega) &= \alpha_{F_n}^{(0)}(\omega) + \alpha_{F_n}^{(1)}(\omega)\frac{A \cos \theta_k M_{F_n}}{2F_n} + \alpha_{F_n}^{(2)}(\omega) \\ &\times \left(\frac{3 \cos^2 \theta_p - 1}{2} \right) \left[\frac{3M_{F_n}^2 - F_n(F_n + 1)}{F_n(2F_n - 1)} \right]. \end{aligned} \quad (2)$$

Here $\alpha_{F_n}^{(i)}(\omega)$ are the scalar, vector and tensor components of the frequency dependent polarizability for $i = 0, 1$, and 2 respectively, A represents degree of polarization, θ_k is the angle between quantization axis and wave vector, and θ_p is the angle between quantization axis and direction of polarization. In the presence of magnetic field, $\cos \theta_k$ and $\cos^2 \theta_p$ can have any values depending on the direction of applied magnetic field. In the absence of magnetic field, $\cos \theta_k = 0$ and $\cos^2 \theta_p = 1$ for the linearly polarized light, where polarization vector is assumed to be along the quantization axis. However it yields $\cos \theta_k = 1$ and $\cos^2 \theta_p = 0$ for the circularly polarized light, where the wave vector is assumed to be along the quantization axis. Here we present results for both polarizations of the light assuming absence of the magnetic field. The component of the polarizability can be expressed as [30, 31]

$$\alpha_{F_n}^{(0)}(\omega) = \alpha_{J_n}^{(0)}(\omega), \quad (3)$$

$$\begin{aligned} \alpha_{F_n}^{(1)}(\omega) &= (-1)^{J_n+F_n+I+1} \begin{Bmatrix} F_n & J_n & I \\ J_n & F_n & 1 \end{Bmatrix} \\ &\times \sqrt{\frac{F_n(2F_n+1)(2J_n+1)(J_n+1)}{J_n(F_n+1)}} \alpha_{J_n}^{(1)}(\omega) \end{aligned} \quad (4)$$

and

$$\begin{aligned} \alpha_{F_n}^{(2)}(\omega) &= (-1)^{J_n+F_n+I} \begin{Bmatrix} F_n & J_n & I \\ J_n & F_n & 2 \end{Bmatrix} \\ &\times \sqrt{\frac{F_n(2F_n-1)(2F_n+1)}{(2F_n+3)(F_n+1)}} \\ &\times \sqrt{\frac{(2J_n+3)(2J_n+1)(J_n+1)}{J_n(2J_n-1)}} \alpha_{J_n}^{(2)}(\omega). \end{aligned} \quad (5)$$

Here, J_n is the total angular momentum of the atomic state, I is the nuclear spin and $\alpha_{J_n}^{(i)}$ for $i = 0, 1, 2$ are the scalar, vector and tensor components of the atomic dipole polarizability which are given by [33]

$$\alpha_{J_n}^{(0)}(\omega) = \frac{2}{3(2J_n + 1)} \sum_{k \neq n} \frac{(E_n - E_k) |\langle J_n || \mathbf{D} || J_k \rangle|^2}{\omega^2 - (E_n - E_k)^2}, \quad (6)$$

$$\begin{aligned} \alpha_{J_n}^{(1)}(\omega) &= \sqrt{\frac{24J_n}{(J_n + 1)(2J_n + 1)}} \sum_{k \neq n} (-1)^{J_n + J_k} \\ &\times \begin{Bmatrix} J_n & 1 & J_n \\ 1 & J_k & 1 \end{Bmatrix} \frac{\omega |\langle J_n || \mathbf{D} || J_k \rangle|^2}{\omega^2 - (E_n - E_k)^2} \end{aligned} \quad (7)$$

and

$$\begin{aligned} \alpha_{J_n}^{(2)}(\omega) &= \sqrt{\frac{40J_n(2J_n - 1)}{3(J_n + 1)(2J_n + 3)(2J_n + 1)}} \sum_{k \neq n} (-1)^{J_n + J_k} \\ &\times \begin{Bmatrix} J_n & 2 & J_n \\ 1 & J_k & 1 \end{Bmatrix} \frac{(E_n - E_k) |\langle J_n || \mathbf{D} || J_k \rangle|^2}{\omega^2 - (E_n - E_k)^2}, \end{aligned} \quad (8)$$

where J_m and E_m are the total angular momentum and energy, respectively, for $m = n, k$ states and $\langle J_n || \mathbf{D} || J_k \rangle$ are the reduced E1 matrix elements.

The BBR shift experienced by a state resulting from radiations with all possible frequencies at a temperature T (in Kelvin (K)) relative to the room temperature can be estimated using the expression [32]

$$\Delta E_F^{BBR} \simeq -\frac{1}{2} (831.9 \text{ V/m})^2 \left[\frac{T(\text{K})}{300} \right]^4 \alpha_F^{(0)}(0) (1 + \eta), \quad (9)$$

where η is the dynamic fractional correction factor and is defined as

$$\eta = \frac{(80/63)\pi^2 T^2}{(J_n + 1)\alpha_F^{(0)}(0)} \sum_k \frac{|\langle J_n || \mathbf{D} || J_k \rangle|^2}{(E_n - E_k)^3} \left(1 + \frac{21\pi^2 T^2}{5(E_n - E_k)^2} + \frac{336\pi^4 T^4}{11(E_n - E_k)^4} \right). \quad (10)$$

The differential BBR shift of a transition is, thus, the difference of the BBR shifts of the states associated with that transition. We use atomic units (a.u.) throughout the article unless stated otherwise. The α_{F_n} values can be converted from a.u. to $\text{Hz m}^2\text{V}^{-2}$ and Jm^2V^{-2} by dividing with factors 2.48832×10^{-8} and 6.064×10^{40} , respectively.

The differential AC-Stark shift for a transition between states with hyperfine moments F and F' is given by

$$\begin{aligned} \delta(\Delta E_{FF'}^{Stark}) &\approx \Delta E_F^{Stark} - \Delta E_{F'}^{Stark} \\ &= -\frac{1}{2} \delta\alpha_{FF'}(\omega) \mathcal{E}^2(\omega). \end{aligned} \quad (11)$$

In order to find out λ_{magic} of a transition, it is imperative to identify the corresponding values of ω at which the differential Stark shift $\delta(\Delta E_{FF'}^{Stark})$ is zero for any finite electric field strength \mathcal{E} . By suitably choosing polarization of the electric field and azimuthal sublevels, λ_{magic} can be determined for different hyperfine levels of a transition. In fact, we had demonstrated in a recent work that by suitably deciding a trap geometry the

Stark shift of an atomic state or differential Stark shift of a transition can be obtained which can be independent of the vector and tensor components of the states involved [43]. Assuming such a trapping configuration can be achieved for trapping the Yb⁺ ion, we also give λ_{magic} for the aforementioned clock transition. This **comprehensive trapping scheme** could be useful for avoiding hyperfine level selective trapping of ¹⁷¹Yb⁺. We also evaluate λ_T values for which $\alpha_F(\omega)$ can become zero independently for the [4f¹⁴6s] ²S_{1/2} and [4f¹⁴5d] ²D_{3/2} states.

3. Method of calculations

We divide contributions to each $\alpha_{J_n}^{(i)}$ component broadly into three parts, as described in Refs. [26, 34], which is expressed as

$$\alpha_{J_n}^{(i)} = \alpha^{(i,c)} + \alpha_{J_n}^{(i,cv)} + \alpha_{J_n}^{(i,v)} . \quad (12)$$

The superscripts c , cv and v in the parentheses are known as core (independent of J_n), core-valence and valence contributions, respectively [26, 34]. When the core of the electron distribution has an inert gas configuration, core and core-valence contributions usually come out to be much smaller than the valence contribution [25, 26, 34, 35]. This has also been observed earlier in the ground state polarizability study of Yb⁺ [35]. Again, it is possible to use the reduced E1 matrix elements among the low-lying bound states directly in Eqs. (6-8) in a sum-over-states approach to estimate the dominant contribution to $\alpha_{J_n}^{(i,v)}$. We refer to this as ‘‘Main’’ valence correlation contribution and the rest that comes from the other higher level excited states as ‘‘Tail’’ contribution to $\alpha_{J_n}^{(i,v)}$.

For accurate determination of the E1 matrix elements between many low-lying states, we employ the relativistic coupled-cluster (RCC) method by expressing the wave function ($|\Psi_v\rangle$) of an atomic state that has the closed core [5p⁶] and a valence orbital v as

$$|\Psi_v\rangle = e^T \{1 + S_v\} |\Phi_v\rangle \quad (13)$$

where $|\Phi_v\rangle$ is a reference state, which is defined as $|\Phi_v\rangle = a_v^\dagger |\Phi_0\rangle$ with the Dirac-Hartree-Fock (DHF) wave function $|\Phi_0\rangle$ of the closed-core, T and S_v are the RCC excitation operators that excite electrons from the core and core along with the valence orbital respectively. In this work, we have only accounted for the single and double excitations which are denoted using the subscripts 1 and 2 respectively in the RCC operators as

$$T = T_1 + T_2 \quad \text{and} \quad S_v = S_{1v} + S_{2v}. \quad (14)$$

These are known as coupled-cluster singles and doubles (CCSD) method in the literature. Amplitudes of these operators are evaluated using the equations

$$\langle \Phi_0^* | \overline{H} | \Phi_0 \rangle = 0 \quad (15)$$

and

$$\langle \Phi_v^* | (\overline{H} - E_v) S_v | \Phi_v \rangle = - \langle \Phi_v^* | \overline{H} | \Phi_v \rangle, \quad (16)$$

Table 1. Contributions to the static values of $\alpha_{J_n}^{(i=0,2)}$ for the $[4f^{14}6s] \ ^2S_{1/2}$ and $[4f^{14}5d] \ ^2D_{3/2}$ states in Yb⁺ are given in a.u. Absolute values of the dominantly contributing reduced E1 matrix elements (in a.u.) and resonance wavelengths in vacuum (λ_{res} in nm) are also listed. Values quoted in bold fonts are taken from other work as mentioned below.

Contribution	λ_{res} [41]	E1	$\alpha_{J_n}^{(0)}$	$\alpha_{J_n}^{(2)}$
$[4f^{14}6p] \ ^2P_{1/2}$	369.52	2.471(3) [36, 37]	16.51(4)	
$[4f^{13}5d6s] \ ^3[3/2]_{3/2}$	347.73	1.10 [38]	3.1	
$[4f^{14}6p] \ ^2P_{3/2}$	329.03	3.36(3) [36, 37]	27.2(5)	
$[4f^{13}5d6s] \ ^3[3/2]_{1/2}$	297.05	0.82(2) [39, 40]	1.46(3)	
$[4f^{13}5d6s] \ ^1[3/2]_{3/2}$	289.14	1.27(2) [39]	3.45(3)	
$[4f^{14}7p] \ ^2P_{1/2}$	156.97	0.08(1)	0.0008(1)	
$[4f^{14}7p] \ ^2P_{3/2}$	152.45	0.11(1)	0.014(2)	
$\alpha^{(i,c)}$			7.7(7)	
$\alpha_{6s^2S_{1/2}}^{(i,cv)}$			-0.16(2)	
Tail($\alpha_{6s^2S_{1/2}}^{(i,v)}$)			0.046(15)	
Total			59.3(8)	
Ref. [35]			62.04	
Ref. [14]			47(9) ^a	
$[4f^{13}5d6s] \ ^3[3/2]_{5/2}$	2632.81	0.00075 [39]	0.0	0.0
$[4f^{14}6p] \ ^2P_{1/2}$	2438.42	2.97(4) [36, 37]	79(2)	-79(2)
$[4f^{13}5d6s] \ ^3[3/2]_{3/2}$	1724.98	0.27 [38]	0.46	0.37
$[4f^{14}6p] \ ^2P_{3/2}$	1345.63	1.31(2)	8.45(26)	6.76(21)
$[4f^{13}5d6s] \ ^3[3/2]_{1/2}$	935.19	0.62(1) [39, 40]	1.31(4)	-1.31(4)
$[4f^{14}7p] \ ^2P_{1/2}$	245.42	0.14(2)	0.018(5)	-0.018(5)
$[4f^{14}7p] \ ^2P_{3/2}$	234.56	0.014(5)	0.0002(1)	0.0001(1)
$[4f^{14}5f] \ ^2F_{5/2}$	210.34	2.43(4)	4.54(15)	-0.91(3)
$[4f^{14}6f] \ ^2F_{5/2}$	173.92	1.47(2)	1.38(4)	-0.275(7)
$[4f^{14}7f] \ ^2F_{5/2}$	158.89	0.93(1)	0.503(11)	-0.101(2)
$[4f^{14}8f] \ ^2F_{5/2}$	151.02	0.35(1)	0.068(4)	-0.014(1)
$\alpha^{(i,c)}$			7.7(7)	0.0
$\alpha_{5d^2D_{3/2}}^{(i,cv)}$			-0.43(3)	-0.08(1)
Tail($\alpha_{5d^2D_{3/2}}^{(i,v)}$)			4(2)	-0.83(25)
Total			107(3)	-75(2)
Ref. [14]			90(17) ^a	
Ref. [16]				-82(13)

^aNote: Estimated by combining measured differential scalar polarizability $\alpha_{6s^2S_{1/2}}^{(0)} - \alpha_{5d^2D_{3/2}}^{(0)}$ from Ref. [16] and E1 matrix elements from the measured lifetimes of many states as listed in Ref. [14].

where $|\Phi_0^*\rangle$ and $|\Phi_v^*\rangle$ are the excited state configurations, here up to doubles, with respect to the DHF states $|\Phi_0\rangle$ and $|\Phi_v\rangle$, respectively, and $\overline{H} = (He^T)_l$ with subscript l representing the linked terms only. E_v is the energy eigenvalue of the $|\Psi_v\rangle$ state and is determined by using the expression

$$E_v = \langle \Phi_v | \overline{H} \{1 + S_v\} | \Phi_v \rangle. \quad (17)$$

Both Eqns. (16) and (17) need to be solved simultaneously for obtaining solutions of interdependent variables in a self-consistent approach. At the same level of approximation in the excitations, a truncated RCC method can incorporate more contributions as compared to a truncated configuration-interaction (CI) method. For example, the lowest order mixing of $[4f^{13}5d6s]^3[3/2]$ with $J = 1/2$ configuration and the DHF wave function of the $[4f^{14}6p]^2P_{1/2}$ configuration is carried out by the S_{2v} operator while calculating the $[4f^{14}6p]^2P_{1/2}$ atomic state function. Similar mixing also takes place among the $J = 3/2$ configurations. Moreover, \overline{H} in the CCSD method contains many non-linear terms that can take into account contributions from the higher level excitations, such as triples and quadruples, at the same level of excitation approximation of the CI method. As a matter of fact, the above mentioned configuration mixing are incorporated through the non-linear terms of the CCSD method and they take care of higher order correlation contributions. This is a unique feature of a truncated RCC method in contrast to other truncated many-body methods owing to the exponential form of expression in Eq. (13). In fact, it has also been employed to calculate many atomic properties of Yb⁺ accurately in the past [6, 12].

After obtaining amplitudes using the above equations, the transition matrix element of the dipole operator D between the states $|\Psi_i\rangle$ and $|\Psi_f\rangle$ is evaluated using the expression

$$\frac{\langle \Psi_f | D | \Psi_i \rangle}{\sqrt{\langle \Psi_f | \Psi_f \rangle \langle \Psi_i | \Psi_i \rangle}} = \frac{\langle \Phi_f | \tilde{D}_{fi} | \Phi_i \rangle}{\sqrt{\langle \Phi_f | \{1 + \tilde{N}_f\} | \Phi_f \rangle \langle \Phi_i | \{1 + \tilde{N}_i\} | \Phi_i \rangle}}, \quad (18)$$

where $\tilde{D}_{fi} = \{1 + S_f^\dagger\} e^{T^\dagger} D e^T \{1 + S_i\}$ and $\tilde{N}_{k=f,i} = \{1 + S_k^\dagger\} e^{T^\dagger} e^T \{1 + S_k\}$. The above expression involves two non-terminating series in the numerator and denominator, which are $e^{T^\dagger} D e^T$ and $e^{T^\dagger} e^T$ respectively, and calculation of these terms are described in our previous works [12]. The “Main($\alpha_{J_n}^{(i,v)}$)” contributions have been calculated by combining the E1 matrix elements obtained using the above expression with the experimental energies as listed in Ref. [41].

Contributions from higher excited states including continuum to $\alpha_{J_n}^{(i,v)}$, denoted as “Tail($\alpha_{J_n}^{(i,v)}$)”, are estimated approximately in the DHF method using the expression

$$\alpha_{J_n}^{(i,v)}(\omega) = \frac{2}{3(2J_n + 1)} \sum_{K > n} \frac{(\epsilon_K - \epsilon_n) |\langle J_n || \mathbf{D} || J_K \rangle_{DHF}|^2}{(\epsilon_n - \epsilon_K)^2 - \omega^2}, \quad (19)$$

where $\langle J_n || \mathbf{D} || J_K \rangle_{DHF}$ are obtained using the DHF wave functions, $K > n$ corresponds to the excited states including continuum whose matrix elements are not accounted in

the Main($\alpha_{J_n}^{(i,v)}$) contribution, and $\epsilon_{n,K}$ refers to the DHF energies.

Similarly, the core-valence contributions $\alpha_{J_n}^{(i,cv)}$ are also obtained through the DHF method approximation using the expression

$$\alpha_{J_n}^{(i,cv)}(\omega) = \frac{2}{3(2J_n + 1)} \sum_K^{N_c} \frac{(\epsilon_K - \epsilon_n) |\langle J_n || \mathbf{D} || J_K \rangle_{DHF}|^2}{(\epsilon_n - \epsilon_K)^2 - \omega^2}, \quad (20)$$

where N_c is the total number of electrons in the closed-core of the Yb^+ . The static scalar core contributions $\alpha^{(0,c)}(0)$ in Yb^+ , which is equal to the ground state polarizability of Yb^{2+} , are evaluated using the DHF, random-phase approximation (RPA) and a perturbed CCSD method considering a dipole operator D as an external perturbation as described in Ref. [42]. The trends in these results demonstrate role of electron correlation effects for its accurate evaluation. The DHF and RPA contributions are subsumed within the CCSD result by the formulation of the theory and are considered as the most precise calculation. Comparison between the DHF and CCSD results than between the RPA and CCSD show small differences between these results while the CCSD method is computationally very expensive. As a matter of fact, it is not possible to apply the CCSD method to determine core contribution to the dynamic polarizabilities for the estimates of the λ_{magic} and λ_{T} values. Therefore, we employ the DHF method to calculate the core contributions to the dynamic polarizabilities. Nevertheless, core contributions cancel out completely in the determination of λ_{magic} . Hence, accuracies in those values are not affected by the use of core correlations from the DHF method while the λ_{T} values can be estimated within reasonable accuracy.

4. Results and Discussion

The obtained static polarizabilities for the $[4f^{14}6s] \ ^2S_{1/2}$ and $[4f^{14}5d] \ ^2D_{3/2}$ states and estimated BBR shifts associated with these states are presented in this section. It can be understood from Fig. 1 that the $[4f^{14}6p] \ ^2P_{1/2,3/2}$ states will contribute dominantly to the polarizabilities of both the ground and $[4f^{14}5d] \ ^2D_{3/2}$ states. Therefore, knowledge of precise E1 matrix elements between these states are crucial in estimating polarizabilities of the above two states associated with the clock transition. After discussing accuracies in the static polarizability results, we move on to presenting the dynamic polarizabilities of the $[4f^{14}6s] \ ^2S_{1/2}$ and $[4f^{14}5d] \ ^2D_{3/2}$ states in Yb^+ and adjudge that these quantities will also have similar accuracies with their corresponding static polarizability values.

4.1. Static polarizability

In Table 1, we give contributions from the individual correlation effects to the static $\alpha_{J_n}^{(i)}$ values of the ground and $[4f^{14}5d] \ ^2D_{3/2}$ states in $^{171}\text{Yb}^+$. The ‘‘Main’’ contributions are listed separately in the table along with the E1 matrix elements and resonant wavelengths λ_{res} of different transitions involving the low-lying $P_{1/2,3/2}$ states to

Table 2. The λ_{magic} values in nm and their corresponding α_{F_n} values in a.u. values among different M_{F_n} sub-levels of the $[4f^{14}6s] \ ^2S_{1/2}(F=0) \rightarrow [4f^{14}5d] \ ^2D_{3/2}(F=2)$ clock transition in $^{171}\text{Yb}^+$ are listed for both the linearly and right-circularly polarized light.

Linear			Circular		
M_F	λ_{magic}	α_{F_n}	M_F	λ_{magic}	α_{F_n}
0	1725.4(1)	62(2)	-2	1726.5(1)	60(5)
	1356.3(3)	63(2)		1381.8(6)	62(2)
	951.8(5)	66(2)		948.9(2)	64(2)
	357.3(1)	21.03(1)		358.1(2)	-6.2(3)
	344.9(1)	21.81(4)		345.2(2)	-5.1(3)
	298.8(3)	25.68(3)		299.1(1)	-1.31(6)
	291.8(1)	26.52(6)		292.2(1)	-0.80(1)
	245.4(1)	-53.43(3)		243.5(1)	-55.3(2)
± 1	1726.6(1)	61(2)	-1	1728.8(3)	61(2)
	1382(1)	63(2)		1418(2)	62(2)
	948(1)	65(2)		944.4(2)	67(3)
	357.3(2)	20.61(3)		357.8(1)	5.7(1)
	344.9(1)	21.01(2)		345.1(1)	6.4(2)
	298.8(1)	24.62(6)		299.0(1)	9.41(5)
	291.8(1)	25.43(5)		292.1(1)	9.89(7)
	245.4(1)	-53.59(6)		0	1735.4(2)
± 2	1788(6)	63(1)	0	1479(5)	62(5)
	1619(5)	59(1)	0	939.7(2)	67(2)
	357.4(2)	18.0(2)	0	357.4(2)	18.8(2)
	345.1(2)	18.42(2)	0	345.0(2)	19.3(3)
	298.8(1)	20.63(5)	0	298.8(1)	21.96(5)
	291.9(1)	21.20(5)	0	291.9(1)	22.50(7)
			1	1657(15)	61(2)
			1	356.9(2)	32.1(6)
		1	344.8(2)	32.5(3)	
		1	298.7(1)	35.30(5)	
		1	291.7(1)	35.84(5)	
		2	1204(45)	64(2)	
		2	356.5(2)	46.6(9)	
		2	344.7(2)	47.0(5)	
		2	298.5(1)	50.31(7)	
		2	291.6(1)	51.17(9)	

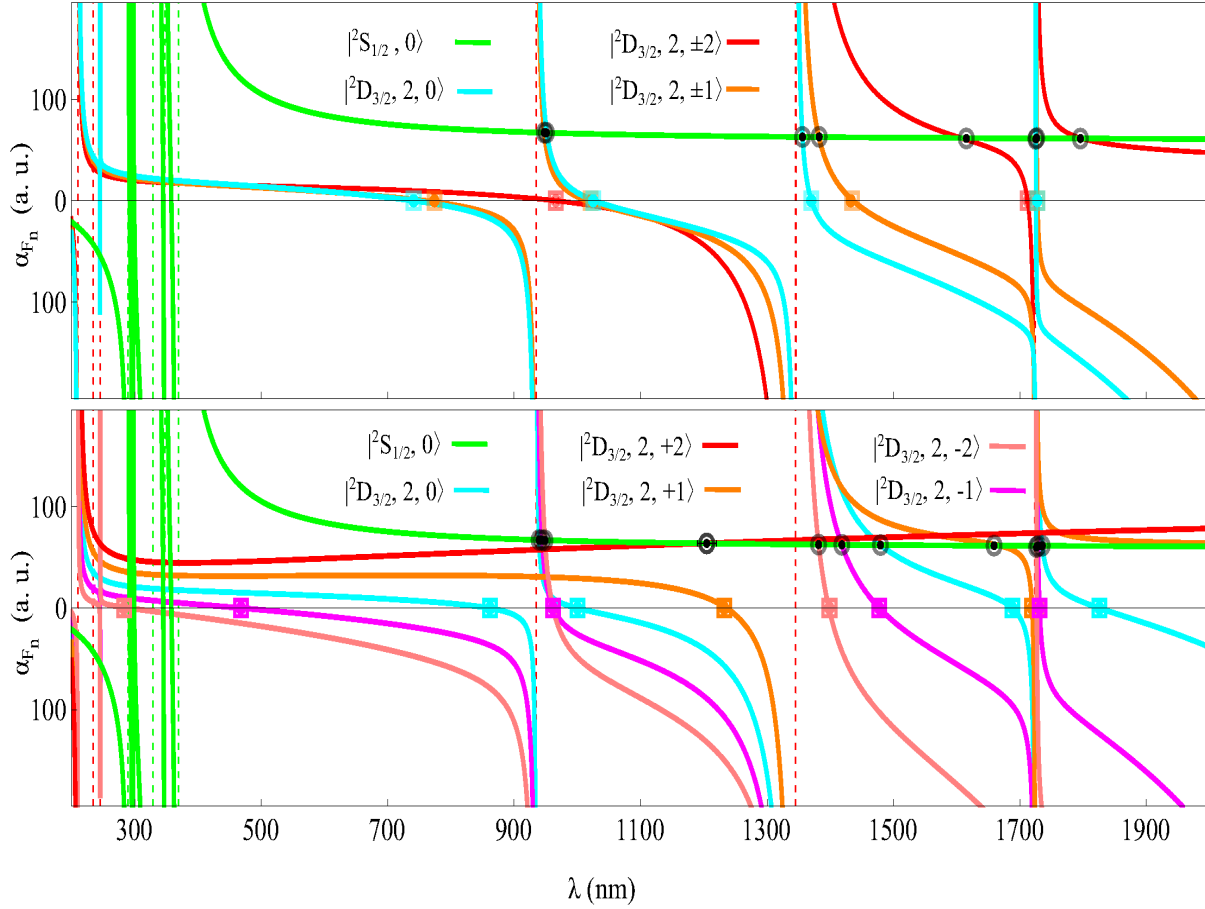


Figure 2. Wavelength dependent dynamic dipole polarizabilities of the $[4f^{14}6s] \ ^2S_{1/2}(F=0)$ state (denoted by $|^2S_{1/2}, 0\rangle$) and for all possible M_F sublevels of the $[4f^{14}5d] \ ^2D_{3/2}(F=2)$ state (denoted by $|^2D_{3/2}, 2, M\rangle$) in $^{171}\text{Yb}^+$ using (a) linearly and (b) right-circularly polarized light. The λ_{magic} and λ_T values are indicated in dots which are encircled by circles and squares, respectively. The vertical dashed lines signify the resonances from the ground and $[4f^{14}5d] \ ^2D_{3/2}(F=2)$ states in green and red colors, respectively.

illustrate their roles explicitly in the accurate evaluation of $\alpha_{J_n}^{(i)}$. Uncertainties of these matrix elements are given along with their respective values. The uncertainties in the CCSD values are determined by estimating contributions from the neglected leading order triple excitations and due to use of the the finite size basis functions in the calculation. We find more than 90% contribution to the total static $\alpha_{J_n}^{(i)}$ values come from the $[4f^{14}6p] \ ^2P_{1/2}$ and $[4f^{14}6p] \ ^2P_{3/2}$ states in both the cases. Thus, we replace the E1 matrix elements of the $[4f^{14}6s] \ ^2S_{1/2} \rightarrow [4f^{14}6p] \ ^2P_{1/2,3/2}$ and $[4f^{14}5d] \ ^2D_{3/2} \rightarrow [4f^{14}6p] \ ^2P_{1/2}$ transitions that are obtained from the CCSD method by the values extracted from the combination of the experimental values of the lifetimes and the corresponding branching ratios from [36, 37] of the $[4f^{14}6p] \ ^2P_{1/2}$ and $[4f^{14}6p] \ ^2P_{3/2}$ states. These values are quoted in bold fonts while the CCSD values are mentioned just below these numbers in Table 1. We, however, could not extract out the E1 matrix

element of the $[4f^{14}5d] \ ^2D_{3/2} \rightarrow [4f^{14}6p] \ ^2P_{3/2}$ transition from any available experimental data. Nevertheless, we find that the experimental value of the E1 matrix element, that is 2.97 a.u., corresponding to the $[4f^{14}5d] \ ^2D_{3/2} \rightarrow [4f^{14}6p] \ ^2P_{1/2}$ transition is very close to our CCSD result (2.95 a.u.). Since the $[4f^{14}6p] \ ^2P_{1/2}$ and $[4f^{14}6p] \ ^2P_{3/2}$ states are the fine structure partners, electron effects will behave similarly in determining these states. Therefore, we assume that the CCSD value for the E1 matrix element of the $[4f^{14}5d] \ ^2D_{3/2} \rightarrow [4f^{14}6p] \ ^2P_{3/2}$ transition will have similar accuracy as of the corresponding value of the $[4f^{14}5d] \ ^2D_{3/2} \rightarrow [4f^{14}6p] \ ^2P_{1/2}$ transition. Next to the $6P$ states, there lie the states with $[4f^{13}5d6s]$ configurations. Finding E1 matrix elements for these states are strenuous in the RCC method, but a CI method can estimate them more reliably. We consider these values either from the experimental data presented in Ref. [39] or are taken from the theoretical calculations reported in Ref. [38] using a CI method. Since uncertainties of these matrix elements obtained from the CI method are not given and their contributions to the polarizability values are found to be relatively small (see Table 1), we have not accounted for uncertainties from these matrix elements in the present work. In order to infer E1 matrix element of the $[4f^{13}5d6s] \ ^3[3/2]_{1/2} \rightarrow [4f^{14}5d] \ ^2D_{3/2}$ transition for estimating its contribution in the evaluation of the polarizability of the $[4f^{14}5d] \ ^2D_{3/2}$ state, we have used the experimentally measured lifetime of the $[4f^{13}5d6s] \ ^3[3/2]_{1/2}$ state from Ref. [39] and branching ratios reported in Refs. [40, 44].

As seen in Table 1, the core correlation has significant contribution to the scalar $\alpha_{J_n}^{(0)}$ values. This cannot be evaluated using a sum-over-states approach, so it is imperative to apply a suitable *ab initio* many-body method for its determination. The core correlation contribution $\alpha^{(i,c)}$ to the ground and $[4f^{14}5d] \ ^2D_{3/2}$ states of Yb⁺, which corresponds to dipole polarizability of the Yb²⁺ ion, has not been evaluated rigorously earlier. To determine this contribution more reliably, we apply three different methods in the DHF, RPA and CCSD approximations based on the first principle calculations as discussed in Ref. [42]. We find $\alpha^{(i,c)} = 7.45$ a.u., $\alpha^{(i,c)} = 6.38$ a.u. and $\alpha^{(i,c)} = 7.72$ a.u. from the DHF, RPA and CCSD methods, respectively. In Ref. [35], the RPA value is given as 6.386 a.u. which agrees well with our RPA value. The DHF value is found to be larger than the RPA value, the CCSD value is larger than the other two methods. Though RPA is also an all order method, but it takes into account only the core-polarization correlations while the CCSD method includes pair-correlation effects to all orders along with the core polarization effects. We, therefore, consider CCSD value as the final result and it is given along with the estimated uncertainty in Table 1.

The ‘‘Tail’’ contributions to $\alpha_{J_n}^{(i,v)}$ and $\alpha_{J_n}^{(i,cv)}$ are also given in Table 1, which are obtained using the DHF method. The core-valence contributions are found to be negligibly small, whereas the ‘‘Tail’’ contributions to the scalar and tensor polarizabilities of the $[4f^{14}5d] \ ^2D_{3/2}$ state are significant. Accounting all these contributions, we obtain the final static polarizability of the ground state as 59.3(8) a.u., while the static scalar and tensor polarizabilities of the $[4f^{14}5d] \ ^2D_{3/2}$ state are 107(3) a.u. and $-75(2)$ a.u., respectively. An earlier calculation using the relativistic many-body perturbation

theory (MBPT) presents ground state static polarizability value as 62.04 a.u.[35]. The discrepancy arises from the value of E1 matrix elements that are used for the transitions involving the $[4f^{14}6p] \ ^2P_{1/2}$ and $[4f^{14}6p] \ ^2P_{3/2}$ states. On the other hand, Lea *et. al.* have also estimated this value as 47(9) a.u. [14] using experimental E1 matrix elements. In their calculation, only few E1 transitions were included and the core contribution was completely neglected. Nevertheless, both the values agree within their respective uncertainties. Accurate calculations of $\alpha_{J_n}^{(i)}$ for the $[4f^{14}5d] \ ^2D_{3/2}$ state is very challenging as compared to the ground state. Here, the E1 matrix elements between this state and the $[4f^{14} \ np] \ ^2P_{1/2,3/2}$ and $[4f^{14} \ nf] \ ^2F_{5/2}$ states, with the principle quantum number n , mainly contribute. We observe from Table 1 that contributions from the E1 matrix elements involving the $[4f^{14} \ nf] \ ^2F_{5/2}$ states converge very slowly as compared to the $[4f^{14} \ np] \ ^2P_{1/2,3/2}$ states with higher n value. We, therefore, consider $n = 5, 6, 7, 8$ for the $[4f^{14} \ nf] \ ^2F_{5/2}$ states and $n = 6, 7$ for the $[4f^{14} \ np] \ ^2P_{1/2,3/2}$ states in the evaluation of “Main” contribution to $\alpha_{J_n}^{(i,v)}$. Among these contributions, the E1 matrix element of the $[4f^{14}5d] \ ^2D_{3/2} \rightarrow [4f^{14}6p] \ ^2P_{1/2}$ transition dominates. The contribution from the $[4f^{14}5d] \ ^2D_{3/2} \rightarrow [4f^{14}6p] \ ^2P_{3/2}$ transition is found to be about ten times smaller than the above transition. This is owing to the fact that its E1 matrix element is almost half while its transition energy is twice larger than the corresponding value of the $[4f^{14}5d] \ ^2D_{3/2} \rightarrow [4f^{14}6p] \ ^2P_{1/2}$ transition. Noticeably contributions from the $[4f^{13}5d6s]$ configurations are non-significant as seen in Table 1. Unlike for the ground state, the “Tail” contribution to $\alpha_{J_n}^{(o)}$ is about 4% of its total value. Thus, the dominant sources of uncertainty in $\alpha_{J_n}^{(o)}$ comes from the “Tail” contribution. Similar trends are also observed in the determination of the static $\alpha_{J_n}^{(2)}$ value of the $[4f^{14}5d] \ ^2D_{3/2}$ state, which are also quoted in Table 1. Lea *et. al.* have estimated its scalar polarizability value as 90(17) a.u. [14] considering only few E1 matrix elements deducing from the experimental lifetime values. The reason for which we believe to obtain more reliable results for α of the ground and $[4f^{14}5d] \ ^2D_{3/2}$ than the previously estimated values is because of use of more accurate values of the E1 matrix elements of the $[4f^{14}5d] \ ^2D_{3/2} \rightarrow [4f^{14}6p] \ ^2P_{3/2}$, $[4f^{14}5d] \ ^2D_{3/2} \rightarrow [4f^{14} \ 5f] \ ^2F_{5/2}$ and $[4f^{14}5d] \ ^2D_{3/2} \rightarrow [4f^{14} \ 6f] \ ^2F_{5/2}$ transitions, and core contribution that are evaluated using our RCC method. An experimental value of the tensor polarizability of the $[4f^{14}5d] \ ^2D_{3/2}$ state has been reported as $-82(13)$ a.u. [16]. From the comparison, we find our estimated value agrees with the experimental result indicating that we are able to produce polarizabilities in the investigates states accurately.

Using the static polarizability values as mentioned above, we estimate the BBR shifts in the ground and $[4f^{14}5d] \ ^2D_{3/2}$ states of Yb^+ as -0.52 Hz and -0.92 Hz, respectively. Further, we evaluate the dynamic corrections to these quantities approximately, using Eq. (10), as -0.0004 Hz and -0.04 Hz in the ground and $[4f^{14}5d] \ ^2D_{3/2}$ states respectively. From this analysis, we obtain the net differential scalar polarizability value of the $[4f^{14}6s] \ ^2S_{1/2} \rightarrow [4f^{14}5d] \ ^2D_{3/2}$ transition as $-7.8(5) \times 10^{-40} \text{ Jm}^2\text{V}^{-2}$ against the available experimental value of $-6.9(1.4) \times 10^{-40} \text{ Jm}^2\text{V}^{-2}$ [16]. This corresponds to the differential BBR shift for the $[4f^{14}6s] \ ^2S_{1/2} \rightarrow$

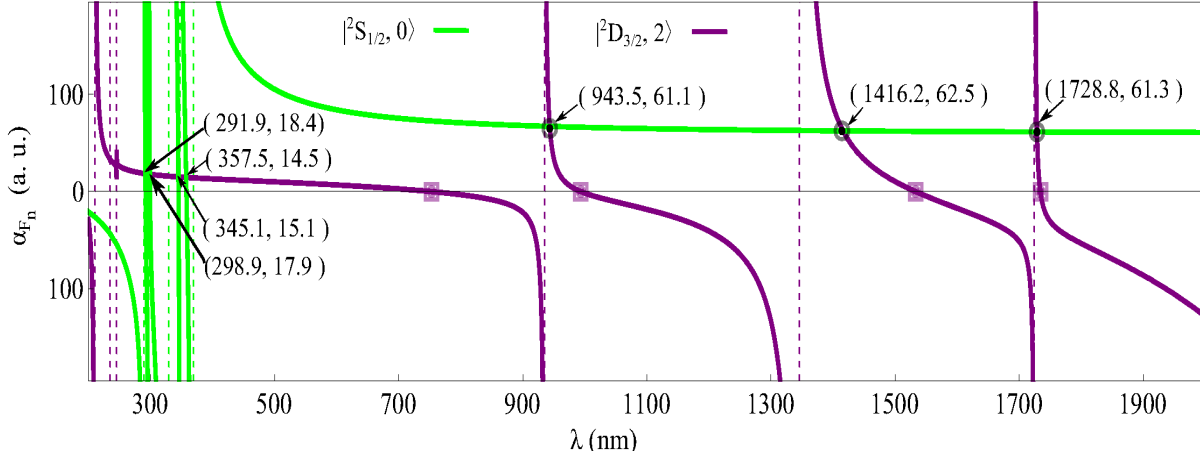


Figure 3. Dynamic scalar polarizabilities of the $[4f^{14}6s] \ ^2S_{1/2}$ and $[4f^{14}6s] \ ^2D_{3/2}$ states when vector and tensor polarizability components are zero. The λ_{magic} and λ_{T} wavelengths for comprehensive trapping are pointed out in dots and encircled by circles and squares, respectively, are independent of the hyperfine levels and magnetic sub-levels of the states. In particular to the λ_{magic} , their corresponding α_F values are indicated within brackets. The vertical dashed lines signify the resonances from the ground and $[4f^{14}5d] \ ^2D_{3/2}$ states in green and purple colors, respectively.

$[4f^{14}5d] \ ^2D_{3/2}$ clock transition as $-0.44(3)$ Hz. This value comes out to be larger than the measured value $-0.37(5)$ Hz by Tamm et al [15], which is being currently considered for estimating uncertainty due to the BBR shift in the above clock transition frequency. There are also two different values were predicted as -0.254 Hz and $-0.261(8)$ Hz by Lea et al from the *ab initio* calculations and combining with both the experimental and theoretical data, respectively [14].

4.2. Magic wavelengths for linearly and circularly polarized light

In order to find out λ_{magic} among different magnetic sublevels M_F of the $[4f^{14}6s] \ ^2S_{1/2}(F = 0) \rightarrow [4f^{14}5d] \ ^2D_{3/2}(F = 2)$ clock transition we estimate dynamic α_{F_n} values of the associated states at different wavelengths ranging from 200-2000 nm. First the atomic polarizabilities of the $[4f^{14}6s] \ ^2S_{1/2}$ and $[4f^{14}5d] \ ^2D_{3/2}$ states are determined using the relations given in Eqs. (6-8), then total polarizability value is obtained from Eq. (2). In Fig.2 we plot our estimated α_{F_n} values of both the states as function of the wavelength. To obtain the λ_{magic} values for the $[4f^{14}6s] \ ^2S_{1/2}, F = 0) \rightarrow [4f^{14}5d] \ ^2D_{3/2}, F = 2)$ transition, we have considered all possible combinations of M_F sublevels and also different light polarizations. In Fig. 2(a), we plot the dynamic polarizabilities for the states associated with the $|^2S_{1/2}, F = 0\rangle \rightarrow |^2D_{3/2}, F = 2, M_F = 0, \pm 1, \pm 2\rangle$ transitions against the wavelength corresponding to a linearly polarized light. Similar plots are shown in Fig. 2(b) for the $|^2S_{1/2}, F = 0\rangle$ and $|^2D_{3/2}, F = 2, M_F = -2, -1, 0, 1, 2\rangle$ states assuming a circular polarized light. **The wavelengths at which intersections of the polarizability curves take place are recognized as λ_{magic} .** In

Table 3. The λ_T values in nm for all possible M_F components of the considered states in $^{171}\text{Yb}^+$ using linearly and right-circularly polarized light. **The term "Both" for $[4f^{14}6s] \ ^2S_{1/2}(F = 0)$ state means that the results are same for linear and circular polarization.**

$[4f^{14}6s] \ ^2S_{1/2}(F = 0)$			$[4f^{14}5d] \ ^2D_{3/2}(F = 2)$					
Polarization	M_F	λ_T	Polarization	M_F	λ_T	Polarization	M_F	λ_T
Both	0	357.9(1)	Linear	0	1725.4(1)	Circular	-2	1726.9(1)
		345.2(1)			1370.2(3)			1398.1(2)
		299.1(1)			1026.9(8)			961.7(1)
		292.2(1)			741.2(5)			283.3(4)
	± 1	1727.8(1)	-1	1731.3(1)				
				1478.1(1)				
				961.6(1)				
				468.2(7)				
	± 2	1712.4(3)	0	1826(2)				
				1688.3(3)				
				1000(2)				
				861(3)				
1	1719.4(1)	2	1233(1)					
			-					

Table 2 we list the λ_{magic} values for the $|4f^{14}6s \ ^2S_{1/2}, F = 0\rangle \rightarrow |4f^{14}5d \ ^2D_{3/2}, F = 2\rangle$ transition in the presence of a linearly polarized light. It can be noticed that these λ_{magic} values support a red-detuned trap (depicted by the positive values of dipole polarizabilities at these wavelengths) except at 245.4 nm. Magic wavelengths at the infrared region are considered to have more experimental significance due to availability of high power fiber or solid state lasers in comparison to ultraviolet wavelengths produced by the sum or difference frequency generation techniques. Similarly, the λ_{magic} for the $|4f^{14}6s \ ^2S_{1/2}, F = 0\rangle \rightarrow |4f^{14}5d \ ^2D_{3/2}, F = 2\rangle$ transition in the presence of a right-circularly polarized light are also given in Table 2. In the present work, we determine λ_{magic} for right circularly polarization using $A = 1$ considering all possible positive and negative M_F sublevels of the states participating in the transition. Note that λ_{magic} for the left circularly polarized light of a transition with a given M_F are equal to right circularly polarized light with opposite sign of M_F .

4.3. Magic wavelengths for comprehensive trapping

In Fig. 3, we show λ_{magic} values that are independent of the hyperfine sub-levels and their M_F sublevels of the states involved in the clock transition. These λ_{magic} values will produce null differential Stark shifts exclusively among any hyperfine level of the ground and excited state. We have identified at least seven magic wavelengths for the hyperfine

level independent trapping, out of which four are in the ultra violet and two in the infra red region. The λ_{magic} values along with the polarizability values at these wavelengths are marked with arrows in Fig. 3. In order to distinguish the M_F independent magic wavelength, the λ_{magic} presented in Table 2 for linearly and circularly polarized light can be compared to the values marked in Fig. 3. The trapping scheme as proposed in Ref. [43] and using λ_{magic} indicated in Fig. 3, one can optically trap Yb^+ with zero light shift in the $[4f^{14}6s] \ ^2S_{1/2} \rightarrow [4f^{14}5d] \ ^2D_{3/2}$ transition for any given combinations of the F and M_F levels that are experimentally viable.

4.4. Tune-out wavelengths

We have identified polarization dependent tune-out wavelengths at which the dynamic polarizabilities reduces to zero individually with different M_F sub-levels in both $F = 0$ state of $[4f^{14}6s] \ ^2S_{1/2}$ and $F = 2$ state of $[4f^{14}5d] \ ^2D_{3/2}$. These λ_T values are listed in Table 3 together with the M_F values against wavelengths of light with linear and circular polarizations. We have also identified four tune-out wavelengths for the $[4f^{14}5d] \ ^2D_{3/2}$ state at 1734.2(2), 1533.2(1), 993.5(5), and 753(3) nm, which could be useful for carrying out measurements irrespective of choice for hyperfine sub-levels.

5. Conclusion

In summary, we have conducted a systematic study of the static polarizabilities for the ground $[4f^{14}6s] \ ^2S_{1/2}$ and metastable $[4f^{14}5d] \ ^2D_{3/2}$ states of Yb^+ . The polarizability values are further used to estimate the BBR shift for the $[4f^{14}6s] \ ^2S_{1/2} \rightarrow [4f^{14}5d] \ ^2D_{3/2}$ transition. The values of the ac polarizabilities are also determined for wavelengths ranging from the ultraviolet through infrared spectral regions, and are used to find out the magic wavelengths for optical trapping of the above mentioned clock transition. These magic wavelengths are given for both the linearly and circularly polarized light and also for a comprehensive trapping scheme which is independent of the hyperfine sub-levels of the states involved in the clock transition. We were also able to identify a number of tune-out wavelengths for the above states. Our results will be of interest for carrying out precision measurements in the $[4f^{14}6s] \ ^2S_{1/2} \rightarrow [4f^{14}5d] \ ^2D_{3/2}$ transition of Yb^+ for attaining high accuracy clock frequency and investigating many fundamental physics.

Acknowledgements

S.D. acknowledges CSIR-National Physical Laboratory, Department of Science and Technology (grant no. SB/S2/LOP/033/2013) and Board of Research in Nuclear Sciences (grant no. 34/14/19/2014-BRNS/0309) for supporting this work. The work of B.A. is supported by Department of Science and Technology, India. B.K.S. acknowledges support under the PRL-TDP program and use of Vikram-100 HPC Cluster at Physical Research Laboratory, Ahmedabad.

References

- [1] M. Roberts *et. al.*, Phys. Rev. A **62**, 020501(R) (2000).
- [2] Chr. Tamm, S. Weyers, B. Lipphardt and E. Peik, Phys. Rev. A **80**, 043403 (2009).
- [3] Y. Imai, K. Sugiyama, T. Nishi, S. Higashitani, T. Momiyama and M. Kitano, Poster No. B3-PWe21 *The 12th Asia Pacific Physics Conference*, 14-19 July 2013.
- [4] A. Rastogi *et. al.*, Mapan **30**, 169 (2015)
- [5] N. Huntemann, C. Sanner, B. Lipphardt, Chr. Tamm, and E. Peik, Phys. Rev. Lett. **116**, 063001 (2016).
- [6] B. K. Sahoo and B. P. Das, Phy. Rev. A **84**, 010502(R) (2011).
- [7] V. A. Dzuba, V. V. Flambaum, and M. V. Marchenko, Phys. Rev. A **68**, 022506 (2003).
- [8] V. A. Dzuba and V. V. Flambaum, Phys. Rev. A **77**, 012515 (2008).
- [9] R. M. Godun *et. al.*, Phys. Rev. Lett. **113**, 210801 (2014).
- [10] V. A. Dzuba, V. V. Flambaum, M. S. Safronova, S. G. Porsev, T. Pruttivarasin, M. A. Hohensee, and H. Haffner, Nat. Phys. **12**, 465 (2016).
- [11] N. Yu and L. Maleki, Phys. Rev. A **61**, 022507 (2000).
- [12] D. K. Nandy and B. K. Sahoo, Phys. Rev. A **90**, 050503(R) (2014).
- [13] N. Batra, B. K. Sahoo and S. De., Chin. Phys. B. **25**, 113703 (2016).
- [14] S. N. Lea, S. A. webster, G. P. Barwood, *Proceeding of the 20th European Frequency and Time Forum (EFTF)*, edited by F. Riehle (PTB, Braunschweig, Germany, 2006), pp. 302-307.
- [15] Chr. Tamm *et. al.*, *Proceeding 20th European Frequency and Time Forum (EFTF)*, edited by F.Riehle(PTB, Braunschweig, Germany, 2006).
- [16] T. Schneider, E. Peik and C. Tamm, Phys. Rev. Lett. **94**, 230801 (2005).
- [17] Pei-Liang Liu, *et. al.* Phys. Rev. Lett. **114**, 223001 (2015).
- [18] Ch. Schnieder, M. Enderleini, and T. Schaetz, Nature. Photonics **4**, 772 (2010).
- [19] Martin Enderlein, Thomas Huber, Christian Schneider, and Tobias Schaetz, Phys. Rev. Lett. **109**, 233004 (2012).
- [20] Shiqian Ding, Huanqian Loh, Roland Hablutzel, Meng Gao, Gleb Maslennikov, and Dzmitry Matsukevich, Phys. Rev. Lett. **113**, 073002 (2014).
- [21] J. Zhang, *et. al.*, Nature **543**, 217 (2017).
- [22] Hidetoshi Katori, Koji Hashiguchi, E. Yu. Ilinova and V. D. Ovsiannikov, Phys. Rev. Lett. **103**, 153004 (2009).
- [23] Andrei Derevianko and Hidetoshi Katori, Rev. Mod. Physics **83**, 331 (2011).
- [24] Z. W. Barber, C. W. Hoyt, C. W. Oates, L. Hollberg, A. V. Taichenachev, and V. I. Yudin, Phys. Rev. Lett. **96**, 083002 (2006).
- [25] Bindiya Arora, M. S. Safronova, and Charles W. Clark, Phys. Rev. A **76**, 052509 (2007).
- [26] Jasmeet Kaur, Sukhjit Singh, Bindiya Arora, and B. K. Sahoo, Phys. Rev. A **92**, 031402 (2015).
- [27] Bindiya Arora, M. S. Safronova, and Charles W. Clark, Phys. Rev. A **84**, 043401 (2010).
- [28] J. A. Sherman, T. W. Koerber, A. Markhotok, W. Nagourney, and E. N. Fortson, Phys. Rev. Lett. **94**, 243001 (2005).
- [29] B. K. Sahoo, L. W. Wansbeek, K. Jungmann, and R. G. E. Timmermans, Phys. Rev. A **79**, 052512 (2009).
- [30] K. Beloy, *Theory of the ac stark effect on the atomic hyperfine structure and applications to microwave atomic clocks* (2009), PhD thesis submitted to University of Nevada, Reno, USA.
- [31] V. A. Dzuba, V. V. Flambaum, K. Beloy, and A. Derevianko, Phys. Rev. A **82**, 062513 (2010).
- [32] S. G. Porsev and A. Derevianko, Phys. Rev. A **74**, 020502(R) (2006).
- [33] N. L. Manakov, V. D. Ovsiannikov, and L. P. Rapport, Phys. Rep. **141**, 319 (1986).
- [34] Bindiya Arora, D. K. Nandy and B. K. Sahoo, Phys. Rev. A **85**, 012506 (2012).
- [35] U. I. Safronova and M. S. Safronova, Phys. Rev. A **79**, 022512 (2009).
- [36] S. Olmschenk, K. C. Younge, D. L. Moehring, D. N. Matsukevich, P.Maunza and C.Monroe, Phys. Rev. A **80**, 022502 (2009)

- [37] E. H. Pinnington, G. Rieger, and J. A. Kernahan, *Phys. Rev. A* **3**, 562421 (1997)
- [38] S. G. Porsev, M. S. Safronova and M. G. Kozlov, *Phys. Rev. A* **86**, 022504 (2012).
- [39] D. Kedzierski, J. Kusz, J. Muzolf, *Spectrochimica Acta Part B.* **65**, 248-252 (2010).
- [40] E. Biemont, J. F. Dutrieux, I. Martin, and P. Quinet, *J. Phys. B* **31**, 3321 (1998).
- [41] NIST atomic spectra Database, [http : //www.nist.gov/pml/data/asd.cfm](http://www.nist.gov/pml/data/asd.cfm)
- [42] Y. Singh, B. K. Sahoo, and B. P. Das, *Phys. Rev. A* **88**, 062504 (2013).
- [43] S. Singh, B. K. Sahoo, and B. Arora, *Phys. Rev. A* **93**, 063422 (2016).
- [44] Hendrik M. Meyer, Matthias Steiner, Lothar Ratschbacher, Christoph Zipkes, and Michael Kohl, *Phys. Rev. A* **85**, 012502 (2012) .